### Title

Redefining Protein Interfaces within Protein Single Crystals with DNA.




### Journal

Journal of the American Chemical Society, 143(23)



### Authors

Partridge, Benjamin

Winegar, Peter

Han, Zhenyu

et al.



### Publication Date

2021-06-16

### DOI

10.1021/jacs.1c04191

Peer reviewed

Published in final edited form as:

*J Am Chem Soc*. 2021 June 16; 143(23): 8925–8934. doi:10.1021/jacs.1c04191.

# Redefining Protein Interfaces within Protein Single Crystals with DNA

**Benjamin E. Partridge**, **Peter H. Winegar**, **Zhenyu Han**, **Chad A. Mirkin**

Department of Chemistry and International Institute for Nanotechnology, Northwestern University, Evanston, Illinois 60208, United States;

## Abstract

Proteins are exquisite nanoscale building blocks: molecularly pure, chemically addressable, and inherently selective for their evolved function. The organization of proteins into single crystals with high positional, orientational, and translational order results in materials where the location of every atom can be known. However, controlling the organization of proteins is challenging due to the myriad interactions that define protein interfaces within native single crystals.Recently, we discovered that introducing a single DNA–DNA interaction between protein surfaces leads to changes in the packing of proteins within single crystals and the protein–protein interactions (PPIs) that arise. However, modifying specific PPIs to effect deliberate changes to protein packing is an unmet challenge. In this work, we hypothesized that disrupting and replacing a highly conserved PPI with a DNA–DNA interaction would enable protein packing to be modulated by exploiting the programmability of the introduced oligonucleotides. Using concanavalin A (ConA) as a model protein, we circumvent potentially deleterious mutagenesis and exploit the selective binding of ConA toward mannose to noncovalently attach DNA to the protein surface. We show that DNA association eliminates the major PPI responsible for crystallization of native ConA, thereby allowing subtle changes to DNA design (length, complementarity, and attachment position) to program distinct changes to ConA packing, including the realization of three novel crystal structures and the deliberate expansion of ConA packing along a single crystallographic axis. These findings significantly enhance our understanding of how DNA can supersede native PPIs to program protein packing within ordered materials.

## Graphical Abstract

**Corresponding Author**: **Chad A. Mirkin** – *Department of Chemistry and International Institute for Nanotechnology, Northwestern University, Evanston, Illinois 60208, United States*; chadnano@northwestern.edu.

Supporting Information

The Supporting Information is available free of charge at https://pubs.acs.org/doi/10.1021/jacs.1c04191.

Synthesis and characterization of DNA glycoconjugates; fluorescence competitive binding assays; summary of crystal screening results and crystallographic data; and additional discussion and figures with details of crystal structures (PDF)

Accession Codes

7MG1, 7MG2, 7MG3, 7MG4, 7MG5, 7MG6, 7MG7, 7MG8, 7MG9, 7MGA, 7MGB, 7MGC, and 7MGD (PDB).

Complete contact information is available at: https://pubs.acs.org/10.1021/jacs.1c04191

The authors declare no competing financial interest.

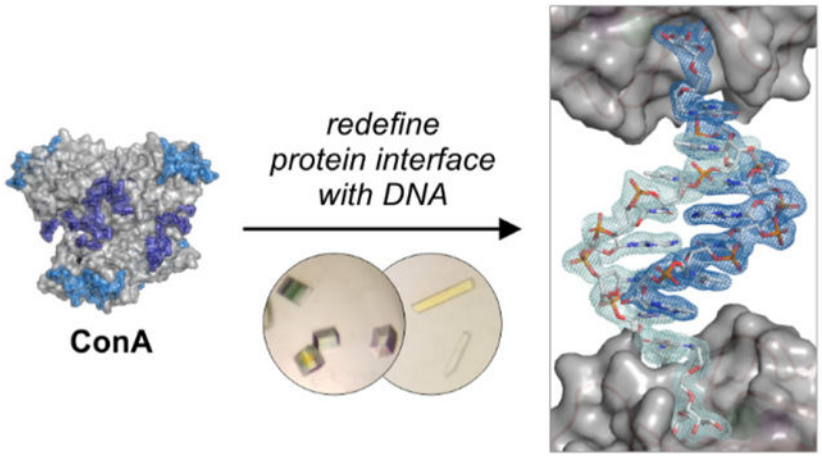


## INTRODUCTION

In Nature, the assembly of proteins into periodic structures enables a multitude of functions, including ordered glycan presentation on bacterial S-layers,[1] structural actuation in muscles,[2] and cargo transport along microtubules.[3] Consequently, synthetic protein assemblies are a promising class of biomaterials that can mimic and surpass the functions of natural protein assemblies.[4–6] Of these, protein single crystals represent assemblies with the greatest degree of positional, orientational, and translational order. This order is desirable for directing energy transfer,[7] controlling catalytic reactions,[8] and harnessing cooperative nanoscale structural changes on the macroscale.[9,10] Understanding the structure–function relationships of these materials, and realizing the full breadth of their potential, requires that the arrangement of proteins can be precisely defined. However, controlling the position and orientation of proteins within single crystals is challenging due to the myriad weak noncovalent interactions on protein surfaces. These native protein–protein interactions (PPIs), which include hydrogen bonding, electrostatics, hydrophobics, and van der Waals, dictate the packing of proteins within single crystals, are difficult to predict, and complicate efforts to program the structural outcome of crystallization.[11,12]

Numerous approaches have been employed to define interactions between proteins and thereby influence crystal packing, including metal coordination,[10,13–18] synthetic symmetrization,[13,19–21] electrostatic programming,[22] computational interface design,[23–27] and supramolecular host–guest binding.[28–32] In many of these strategies, recognition sites must be engineered directly into the protein's amino acid sequence via mutagenesis, which is potentially deleterious to a protein's structure and function. Furthermore, changing the nature of the interaction between protein building blocks necessitates the design and expression of new protein mutants. Therefore, directing crystallization to a different structural outcome by reprogramming these synthetic interactions cannot be done independently of protein design.

DNA has emerged as a powerful ligand to organize nanoscale matter by programming interactions that are agnostic to the nature of the nanoscale building block.[33–39] Over the past decade, the programmability of DNA has been harnessed to organize proteins

into colloidal crystals[40–44] and other hybrid nanostructures.[45–50] Recently, we showed that protein–DNA conjugates containing a single, covalently attached DNA ligand assemble into protein single crystals suitable for X-ray diffraction studies.[51] We found that the introduction of a DNA–DNA interaction can influence the way a protein packs within a crystal because it ultimately changes the exposed protein surface and the nature of the PPIs that arise. Hence, DNA design could be used to modulate structures to some extent. However, to control the packing of proteins within single crystals independently from the design of the protein itself, one must understand how to use programmable interactions, such as DNA, to deliberately disrupt, augment, or replace native PPIs.

We hypothesized that disrupting and replacing a specific, highly conserved PPI by introducing a DNA ligand to the protein surface would enable protein packing to be finely and deliberately modulated using DNA design, leading to more predictable structural outcomes. To investigate this hypothesis, we selected concanavalin A (ConA), a homotetrameric carbohydrate-binding protein (that is, a lectin)[52] whose crystal structure[53] is dominated by a single unique PPI between two recognition sites, one on the face of the protein and one on the vertex of the protein as defined by surface amino acids surrounding the carbohydrate-binding site (Scheme 1a). We envisaged that the noncovalent association of ConA and DNA via carbohydrate binding at that site would sterically block the native PPI recognition site and thus allow crystallization to be programmed using the DNA sequence. Through this approach, based entirely on supramolecular interactions,[4,54,55] we investigate the effect of DNA design parameters including interaction strength, complementarity, sequence length, and attachment position. We show that, by replacing a specific PPI with a DNA–DNA interaction, ConA can be crystallized into five distinct crystal packings and, notably, that changes to the protein packing, including the expansion of ConA packing along a single crystallographic axis, can be programmed via discrete changes to the DNA design. The differences between these structures can be correlated directly with the input DNA design, informed by protein–protein interface analysis and crystallographic elucidation of the oligonucleotide structure. These findings reveal that DNA can eliminate native PPIs within a protein single crystal and thereby enable deliberate changes to protein packing through oligonucleotide sequence design.

## RESULTS AND DISCUSSION

### Design of DNA Glycoconjugates for Noncovalent Attachment of DNA to ConA.

ConA is a homotetrameric lectin that offers several advantages as a model protein for this study. First, ConA and its complexes readily crystallize and have been thoroughly characterized crystallographically, with over 80 entries in the Protein Data Bank (PDB) as of April 2021.[56] Second, its native packing into single crystals is dominated by a single PPI, defined in part by surface amino acids surrounding the carbohydrate-binding site (Scheme 1a). Third, ConA strongly and selectively binds mannose,[52] providing a suitable small molecule to mediate protein– DNA association. Finally, its tetrameric structure adopts a near-tetrahedral geometry ($D_2$ symmetry) whereby four carbohydrate binding sites are positioned at its vertices (Scheme 1a, left). We hypothesized that this geometry would enable binding of multiple DNA ligands at well-defined positions that disrupt native PPIs at the

vertex recognition site (Scheme 1a, right). These advantages have been utilized in previous studies of ligand-induced ConA crystallization, albeit mediated by nonprogrammable hydrophobic interactions.[32,57–60]

To attach DNA noncovalently to ConA via sugar binding, a mannose–DNA conjugate was developed using squaramide chemistry (Schemes 1b and S1). Squaramide linkages have been used extensively to conjugate biomolecules due to their high reaction rate, simple functional group requirements (two primary amines are conjugated together), and the pH dependence of their reactivity, which enables nonsymmetric squaramides to be synthesized by controlling the pH of the conjugation reaction.[61–64] The synthesis of sugar–DNA conjugates is presented in detail in the Supporting Information (Scheme S1 and Figures S1–S18). In brief, an aminefunctionalized mannose derivative (**Man-6**) was reacted with methyl squarate (**7**) to give a mannose–squaramide conjugate (**Man-8**). **Man-8** was subsequently reacted with oligonucleotides containing an aliphatic primary amine (**9**) that were synthesized using standard solid-phase phosphoramidite chemistry (Schemes S2 and S3). The resulting DNA glycoconjugates (Man-DNA, **10**) were purified by reverse-phase high-performance liquid chromatography (RP-HPLC), characterized by matrix-assisted laser-desorption ionization time-of-flight mass spectrometry (MALDI-TOF MS), and quantified by UV–vis spectroscopy (Figures S19 and S20). Sequences and analytical data of all oligonucleotides and DNA glycoconjugates in this study are provided in Table S1. Binding of mannose–DNA conjugates by ConA was confirmed by fluorescence competitive binding assays (Figure S21 and SI Section 3).[65,66]

## DNA Association Eliminates the Major Native PPI of ConA.

Mixtures of ConA and DNA glycoconjugates were screened for crystallization (Scheme 1b) at 22 °C using the sitting-drop vapor-diffusion technique[67] with the Helix conditions screen,[68] which is optimized for nucleic acids and their complexes with proteins. For all structures discussed herein, crystals were obtained in multiple conditions with the same space group and near-identical unit cell parameters (Table S2). Models were built and refined for the highest-resolution diffraction data for each structure (Tables 1 and S3–S5). Full details are provided in SI Section 4.

To determine whether the native dominant PPI is conserved under these conditions, ConA was crystallized in the absence of DNA glycoconjugates, yielding crystals with a cubic morphology in the space group *I*22 (structure I, Figure 1a; PDB: 7MG1). This structure is nearly identical to over 20 PDB entries for native ConA, with a root-mean-square deviation (rmsd) of 0.4 Å for all atoms from a typical ConA structure (PDB: 1JBC[53]). This suggests that, under these conditions, the native PPIs are sufficient to induce crystallization in the absence of DNA. In structure I, an interface exists between the vertices of a given ConA tetrahedron and the faces of surrounding ConA tetramers (Scheme 1a, right, and Figure 1a, left). This interaction leads to staggered sheets of ConA in the *a*–*c* plane (Figure 1a, center) that pack to give a staggered arrangement along the *b*-axis (Figure 1a, right).

To assess how introducing a DNA glycoconjugate would disrupt the targeted PPI during crystallization, a mixture of ConA and Man-ATAT, a self-complementary DNA sequence with mannose attached to the 5′-end (terminus) of the oligonucleotide 5′-ATAT-3′, was

screened for crystallization. Crystals with thin plate morphology were observed and their structures were solved in the space group $P2_122_1$ at 2.10 Å resolution (structure II, Figure 1b; PDB: 7MG5). Notably, the unit cell parameters (Table 1) and space group differ from all previously reported ConA structures, indicating a novel packing. Whereas, in structure I, the mannose-binding sites are involved in PPIs with the faces of other ConA tetramers, these vertices are oriented toward each other in pairs within structure II, suggesting that pairs of oligonucleotides are interacting and thus reprogramming the crystallization of ConA. Unlike the porous packing of structure I, the DNA interactions result in tetramers packing into a brickwork-like arrangement within defined sheets (Figure 1b, center) that repeat with perfect registry in the *b*-direction (Figure 1b, right). The distance between these sheets along the *b*-axis, as measured between the C$\alpha$ atoms of D78 in neighboring tetramers, is ~17 Å (Figure 1b, right, and Figure S22a).

Although a novel crystal structure was observed in the presence of Man-ATAT, we sought to confirm that specific binding of the DNA glycoconjugate via the mannose moiety was responsible for directing the crystal packing of ConA in structure II. Therefore, control experiments were set up in which ConA was mixed with either **Man-8** (that is, the mannose–squaramide without DNA conjugation), 5′-ATAT-3′ (that is, DNA without mannose conjugated), or Gal-ATAT (a DNA glycoconjugate with galactose, which does not appreciably bind to ConA; Figure S21).[52] In all cases, cubic crystals in space group *I*222 with structure I, identical to ConA alone, were observed (Table 1; PDB: 7MG2, 7MG3, 7MG4, respectively). This observation suggests that the presence of neither the sugar nor the DNA alone is sufficient to direct the crystal packing; rather, the specific interaction between ConA and a mannose–DNA conjugate is required.

### Formation of Structure II Depends on DNA Hybridization.

Having established that structure II relies on the binding of an intact mannose–DNA conjugate, we investigated whether the presence of a bound mannose–DNA conjugate is sufficient for crystallization, or whether the formation of structure II requires DNA hybridization. ConA was screened for crystallization in the presence of three additional self-complementary sequences with increasing interaction strength (Man-AGCT, Man-GTAC, and Man-GCGC) as well as a noncomplementary sequence (Man-TTTT). All three self-complementary sequences gave crystals isostructural with Man-ATAT (structure II, Figure 1b and Table 1; PDB: 7MG6, 7MG7, 7MG8, respectively). Excitingly, crystals of ConA and Man-AGCT diffracted to higher resolution (1.70 vs 2.10 Å for Man-ATAT), allowing unambiguous assignment of a four-base-pair (4-bp) DNA double helix in the crystal structure (Figure 2a) that bridges sheets of proteins along the *b*-axis of the unit cell (Figure 1b, left and right). Additionally, unmodeled electron density in the structures with the other 4-bp self-complementary DNA glycoconjugates was consistent with the presence of a 4-bp double-stranded DNA (Figure S23). These structures represent, to the best of our knowledge, the first examples of colloidal crystals engineered with DNA in which the oligonucleotides are sufficiently ordered for their structure to be elucidated crystallographically.

In contrast, crystallization attempts with Man-TTTT did not yield any diffraction-quality crystals. We hypothesized that ConA binds to Man-TTTT, eliminating the native PPI, and thereby inhibiting crystallization because the eliminated PPI was not compensated by DNA hybridization. To test this hypothesis, ConA was crystallized with an equimolar mixture of Man-TTTT and its complement, Man-AAAA. We note that attaining a favorable crystal packing, while ensuring that each bound DNA glycoconjugate hybridizes to its complement, is more challenging with a complementary vs self-complementary DNA design. Indeed, fewer crystals were observed for the crystallization of ConA with Man-TTTT and Man-AAAA, but those that did form possessed structure II (PDB: 7MG9). Electron density was observed for a 4-bp double helix in the same location as in the crystals with self-complementary DNA (Figure S23e). The formation of crystals with a mixture of Man-TTTT and Man-AAAA contrasts with the inability of Man-TTTT to crystallize alone, confirming the role of DNA hybridization in crystallization. Together with the analysis of structures I and II, these findings show that the novel packing of ConA in structure II is driven by both binding of the DNA glycoconjugate via the mannose moiety and hybridization of (self-)complementary oligonucleotides.

### Increasing DNA Length Directly Increases the Distance between Proteins.

Previous work on colloidal crystal engineering with DNA has shown that the length of the oligonucleotides is a powerful design parameter to precisely control structural outcomes.[35] In contrast, realizing the same control over proteins in crystals has so far been elusive; increasing the DNA length of covalent protein–DNA conjugates from 6-bp to 9-bp led to crystallization in a different space group.[51] To examine the effect of DNA length in our current system, ConA was crystallized with a self-complementary 6-bp design, Man-AAATTT. Crystals grew readily and were solved in the $P2_122_1$ space group (structure III, Figure 1c; PDB: 7MGA; $a, b, c$ = 65.1, 77.8, 126.1 Å). Comparison with the unit cell of structure II with Man-ATAT ($a, b, c$ = 65.7, 70.7, 125.9 Å) suggests that the unit cell is expanded along the $b$-direction by ~7 Å. Indeed, examining the crystal structures of structures II and III (Figure 1b,c) shows that ConA packs into identical sheets in the $a$–$c$ plane with an increase in the distance between sheets along the $b$-direction (17 vs 24 Å).

The 2.00 Å resolution electron density maps of structure III show electron density corresponding to a double helix of BDNA (Figure 2b). Notably, comparison of the model for Man-AAATTT with the 4-bp DNA glycoconjugates shows that the 6-bp DNA adopts a near-identical conformation to the 4-bp DNA and is simply extended by 2-bp (Figure 2a vs 2b). This 2-bp extension leads to an expansion of the crystal structure unit cell along the $b$-direction of ~7 Å (Figure S22b), consistent with the expected 3.4 Å rise per bp.[69] Crystallization of ConA with a self-complementary 8-bp DNA (Man-AAAATTTT) was attempted, but no crystals were observed. Nevertheless, comparison of structures II and III demonstrates that changing the DNA length programs a discrete change in the protein packing of ConA that can be directly correlated with the molecular design of the oligonucleotides. We propose that by eliminating the dominant PPI between ConA tetramers, fewer options remain for the protein to explore with respect to reorganizing and forming different PPIs during crystallization, thereby allowing DNA design to program discrete structural changes.

### Attaching Mannose to DNA at an Internal vs Terminal Position Substantially Alters Protein Packing.

Having observed that increasing the DNA length influenced crystal structure, we hypothesized that changing the structure of the DNA ligand would affect its ability to disrupt the native PPI recognition region around the mannose-binding site. Accordingly, DNA glycoconjugates were prepared in which the attachment position of mannose was moved from a terminal position (Man-ATAT) to an internal position (A(Man-T)AT) by conjugating **Man-8** with oligonucleotides synthesized with an amino-modifier C2 dT phosphoramidite (Scheme S2 and Table S1). Crystallizing ConA with A(Man-T)AT or G(Man-T)AC yielded crystals in the space group $P22_12_1$ (structure IV, Figures 3a and S24; PDB: 7MGB, 7MGC). In structure IV, mannose-binding sites from four separate ConA tetramers are oriented toward distinct regions of solvent space (Figure 3a, left). This contrasts with structures II and III, in which binding sites are directed toward each other in pairs, connected by a DNA double helix (Figure 1b,c), and differ from reported structures with similar unit cell dimensions (for example, PDB: 5CNA[70]), in which binding sites are directed toward the faces of adjacent tetramers (Figure S25). Unfortunately, the crystal structures determined for A(Man-T)AT or G(Man-T)AC show electron density only for the mannose moiety. The lack of electron density for the DNA likely arises from disorder, perhaps due to linker flexibility or the formation of multiple binding motifs (Figure S26). Nevertheless, the observation of a distinct crystal packing, confirmation of mannose binding by electron density, and reorientation of mannose-binding sites strongly suggest that DNA hybridization mediates the formation of structure IV.

This conclusion is further supported by the observation of a different structure for the crystallization of ConA with noncomplementary, internally modified T(Man-T)TT (structure V, Figures 3b and S27; PDB: 7MGD). Structure V is nearly identical to complexes of ConA with trisaccharide analogues (PDB: 1ONA[71] and 3D4K;[72] rmsd = 0.6 and 0.7 Å, respectively) and mannose-functionalized octasilsesquioxane clusters (PDB: 3QLQ;[73] rmsd = 0.5 Å), suggesting that T(Man-T)TT acts simply as a sterically blocking group that disrupts the native PPI. Together, structures IV and V reveal that moving the DNA attachment position from a terminal to an internal position—a change of only 1 bp along the DNA backbone—substantially alters the crystal packing of ConA.

### Interface Analysis Allows Correlation of Crystal Packing and DNA Design.

One of the overarching goals in the field of nanoscale assembly is to rationally program structural outcomes through an understanding of assembly processes. For protein assembly in particular, the complex interplay of native PPIs and introduced interactions (here, DNA–DNA and protein–glycoconjugate) limits our ability to program structural outcomes. To understand how a designed DNA–DNA interaction interferes with a specific PPI, we analyzed the interfaces within structures I to V using the PDB's electronic Protein Interfaces, Surfaces, and Assemblies tool[74] (PDBePISA, Figures 4 and S25). For all structures, intratetramer interfaces (that is, interfaces between monomers that define the tetrameric structure) were highly conserved and are thus omitted from the discussion below.

Interface analysis of structure I, containing ConA with no DNA glycoconjugate, confirmed that the primary intertetramer interface exists between the vertex of one tetramer and the face of another tetramer (Figure 4a, dark and light blue, respectively). The amino acids on the vertex that engage in this interaction surround the mannose-binding pocket (Figures 4a and S28). PDB structures nearly identical to structure I suggest that small ligands (for example, dimannose[75] or a tripeptide[76]) can occupy the binding pocket without disrupting the crystal packing. However, the binding of larger ligands, such as the DNA glycoconjugates used here, sterically blocks these residues (Figure 4b, red).

Binding of a DNA glycoconjugate therefore eliminates the major PPI in the native ConA structure and prevents that PPI from directing crystal packing. Crystallization can only proceed if other interactions, including PPIs or designed interactions such as DNA–DNA hybridization, are favorable and can compensate for the lost PPI. Crystals of ConA with noncomplementary T(Man-T)TT (structure V, Figure 3b) do not benefit from DNA hybridization, and therefore, emergent PPIs must compensate for the major PPI eliminated by binding of the DNA glycoconjugate. Interface analysis of structure V (Figure 4c) reveals the presence of three orthogonal sets of emergent PPIs: two sets of PPIs at interfaces between tetramers within a sheet in the *a*–*c* plane (Figure 4c, orange and green) and a third set at the interface between adjacent proteins along the *b*-direction (Figure 4c, blue arrows). This third interface is defined by amino acid residues that are not involved in ConA–ConA interactions in the native structure I (Figure 4a and d, left).

In contrast, the binding of (self)-complementary DNA glycoconjugates introduces the possibility for a new, highly enthalpically favorable interaction within the protein crystal structure: DNA hybridization. Models for structures II and III show that the PPI along the *b*-direction in structure V (blue in Figure 4d, left) can be selectively replaced by a specific DNA– DNA interaction (blue in Figure 4d, center and right). The favorable PPIs at interfaces within the *a*–*c* plane (Figure 4c, orange and green) are maintained, as indicated by the near-identical unit cell parameters *a* and *c* (Table S1), thereby enforcing directionality to the introduced DNA interaction. This directionality is supported by the increasing *b*-parameter across structures V, II, and III (Figure 4d and Table 1). In particular, the expansion of the crystal structure unit cell along the *b*-direction of ~7 Å between structures II and III (Figure 4d, center and right) correlates to a rise of 3.4 Å/bp,[69] highlighting the ability to use DNA to program deliberate changes in protein packing.

Moving the sugar attachment position by 1 bp, from a terminal to an internal position, had a large effect on crystal packing. For noncomplementary strands (Man-TTTT vs T(Man-T)TT), only the internally modified strand was able to induce crystallization, yielding structure V as discussed above. For self-complementary strands (Man-ATAT vs A(Man-T)AT), the change from a terminal to internal modification dramatically changed protein packing (structure II, Figure 1b vs structure IV, Figures 3a and S24). Interface analysis reveals that, while binding of Man-ATAT (structure II) completely eliminates the major native PPI, A(Man-T)AT (structure IV) only partially blocks the amino acid residues at this native interface (Figure S25c), leading to a distinct packing driven by DNA hybridization and additional emergent PPIs. The incomplete blocking of native PPIs in structure IV and

the emergence of PPIs in structures II to V (Figures 4c and S25c) highlight why designing synthetic interactions to override native PPIs is such a formidable challenge.

Fortunately, interface analysis of structures I to V reveals the multiple roles of DNA within protein crystals, thereby highlighting its vast potential as a programmable interaction for protein crystal engineering. By tuning sequence design, DNA glycoconjugates completely inhibited crystallization (Man-TTTT), completely and partially eliminated native PPIs (Man-ATAT vs A(Man-T)AT), facilitated the emergence of PPIs not involved in native packing (structures II, III, and V), selectively overrode emergent PPIs via DNA hybridization (structure II vs structure V), and directed changes in protein packing without disruption to any PPIs (structure III vs structure II).

## CONCLUSION

This work presents a powerful new approach to redefining the interactions between proteins within single crystals using programmable DNA ligands. Indeed, DNA length, complementarity, and attachment position are valuable design handles for modulating protein structure. Crucially, interface analysis reveals that a specific, introduced DNA–DNA interaction can program an expansion of the crystal unit cell along a single crystallographic axis (*b*-direction), with sufficient order that the crystal structure of DNA ligands can be determined. A central goal of the field of programmed protein assembly is being able to redefine the interactions between proteins toward novel, synthetic materials. The squaramide conjugation strategy employed here can be easily modified for the conjugation of DNA to other small molecules, such as enzyme cofactors or drug molecules, providing a route to noncovalent functionalization of other proteins with DNA without the requirement for deleterious mutagenesis. As such, this synthetic approach will enable precise control over the assembly of native proteins into ordered biomaterials. Furthermore, this work represents a major step forward in our understanding of how DNA can eliminate, augment, and replace native PPIs to program protein packing within single crystals. The broad range of roles for DNA within protein crystals raises the possibility of using multiple orthogonal DNA–DNA interactions to achieve unprecedented control over protein assembly pathways and structural outcomes, for the design and synthesis of novel catalystic, energy transporting, and mechanically responsive materials.

## Supplementary Material

Refer to Web version on PubMed Central for supplementary material.

## ACKNOWLEDGMENTS

This material is based upon work supported by the Vannevar Bush Faculty Fellowship program sponsored by the Basic Research Office of the Assistant Secretary of Defense for Research and Engineering and funded by the Office of Naval Research through Grant N00014-15-1-0043, the Air Force Office of Scientific Research under Award FA9550-16-1-0150, and the National Science Foundation under award DMR-2104353. The authors thank Pamela Focia (Northwestern University) for training and advice on macromolecular crystallography; Elena Kondrashkina, Spencer Anderson, and Joseph Brunzelle (Argonne National Laboratory) for assistance with X-ray data acquisition; and Oliver Hayes and Sara Rupich (Northwestern University) for scientific discussions and editorial input. This research used resources of the Advanced Photon Source, a U.S. Department of Energy (DOE) Office of Science User Facility operated for the DOE Office of Science by Argonne National Laboratory under Contract No. DEAC02-06CH11357. Use of the LS-CAT Sector 21 was supported by the Michigan Economic

Development Corporation and the Michigan Technology Tri-Corridor (Grant 085P1000817). This work made use of the IMSERC NMR and MS facilities at Northwestern University, which have received support from the Soft and Hybrid Nanotechnology Experimental (SHyNE) Resource (NSF ECCS-2025633), the State of Illinois, and the International Institute for Nanotechnology (IIN). This work also used resources of the Northwestern University Structural Biology Facility, which is generously supported by the NCI CCSG P30 CA060553 grant awarded to the Robert H. Lurie Comprehensive Cancer Center.

## REFERENCES

(1). Sleytr UB; Schuster B; Egelseer EM; Pum DS-Layers: Principles and Applications. FEMS Microbiol. Rev2014, 38, 823–864. [PubMed: 24483139]

(2). Gotti C; Sensini A; Zucchelli A; Carloni R; Focarete MLHierarchical Fibrous Structures for Muscle-inspired Soft-actuators: A Review. Appl. Mater. Today2020, 20, 100772.

(3). Bachand GD; Spoerke ED; Stevens MJMicrotubule-Based Nanomaterials: Exploiting Nature's Dynamic Biopolymers. Biotechnol. Bioeng2015, 112, 1065–1073. [PubMed: 25728349]

(4). Luo Q; Hou C; Bai Y; Wang R; Liu JProtein Assembly: Versatile Approaches to Construct Highly Ordered Nanostructures. Chem. Rev2016, 116, 13571–13632. [PubMed: 27587089]

(5). Wilson CJ; Bommarius AS; Champion JA; Chernoff YO; Lynn DG; Paravastu AK; Liang C; Hsieh MC; Heemstra JMBiomolecular Assemblies: Moving from Observation to Predictive Design. Chem. Rev2018, 118, 11519–11574. [PubMed: 30281290]

(6). Kuan SL; Bergamini FRG; Weil TFunctional Protein Nanostructures: A Chemical Toolbox. Chem. Soc. Rev2018, 47, 9069–9105. [PubMed: 30452046]

(7). Koshiyama T; Shirai M; Hikage T; Tabe H; Tanaka K; Kitagawa S; Ueno TPost-Crystal Engineering of Zinc-Substituted Myoglobin to Construct a Long-Lived Photoinduced Charge-Separation System. Angew. Chem., Int. Ed2011, 50, 4849–4852.

(8). Tabe H; Abe S; Hikage T; Kitagawa S; Ueno TPorous Protein Crystals as Catalytic Vessels for Organometallic Complexes. Chem. - Asian J2014, 9, 1373–1378. [PubMed: 24677803]

(9). Suzuki Y; Cardone G; Restrepo D; Zavattieri PD; Baker TS; Tezcan FASelf-Assembly of Coherently Dynamic, Auxetic, Two-Dimensional Protein Crystals. Nature2016, 533, 369–373. [PubMed: 27135928]

(10). Bailey JB; Tezcan FATunable and Cooperative Thermomechanical Properties of Protein–Metal–Organic Frameworks. J. Am. Chem. Soc2020, 142, 17265–17270. [PubMed: 32972136]

(11). Derewenda ZS; Vekilov PGEntropy and Surface Engineering in Protein Crystallization. Acta Crystallogr., Sect. D: Biol. Crystallogr2006, 62, 116–124. [PubMed: 16369101]

(12). Derewenda ZS; Godzik AThe "Sticky Patch" Model of Crystallization and Modification of Proteins for Enhanced Crystalliz-ability. In Protein Crystallography: Methods and Protocols; Wlodawer A, Dauter Z, Jaskolski M, Eds.; SpringerNew York: New York, NY, 2017; pp 77–115.

(13). Laganowsky A; Zhao M; Soriaga AB; Sawaya MR; Cascio D; Yeates TOAn Approach to Crystallizing Proteins by Metal-Mediated Synthetic Symmetrization. Protein Sci2011, 20, 1876–1890. [PubMed: 21898649]

(14). Brodin JD; Ambroggio XI; Tang C; Parent KN; Baker TS; Tezcan FAMetal-Directed, Chemically Tunable Assembly of One-, Two- and Three-Dimensional Crystalline Protein Arrays. Nat. Chem2012, 4, 375–382. [PubMed: 22522257]

(15). Sontz PA; Bailey JB; Ahn S; Tezcan FAA Metal Organic Framework with Spherical Protein Nodes: Rational Chemical Design of 3D Protein Crystals. J. Am. Chem. Soc2015, 137, 11598–11601. [PubMed: 26305584]

(16). Zhang L; Bailey JB; Subramanian RH; Tezcan FAHyperexpandable, Self-Healing Macromolecular Crystals with Integrated Polymer Networks. Nature2018, 557, 86–91. [PubMed: 29720635]

(17). Churchfield LA; Tezcan FADesign and Construction of Functional Supramolecular Metalloprotein Assemblies. Acc. Chem. Res2019, 52, 345–355. [PubMed: 30698941]

(18). Golub E; Subramanian RH; Esselborn J; Alberstein RG; Bailey JB; Chiong JA; Yan X; Booth T; Baker TS; Tezcan FAConstructing Protein Polyhedra via Orthogonal Chemical Interactions. Nature2020, 578, 172–176. [PubMed: 31969701]

(19). Banatao DR; Cascio D; Crowley CS; Fleissner MR; Tienson HL; Yeates TOAn Approach to Crystallizing Proteins by Synthetic Symmetrization. Proc. Natl. Acad. Sci. U. S. A2006, 103, 16230–16235. [PubMed: 17050682]

(20). Forse GJ; Ram N; Banatao DR; Cascio D; Sawaya MR; Klock HE; Lesley SA; Yeates TOSynthetic Symmetrization in the Crystallization and Structure Determination of CelA from Thermotoga Maritima. Protein Sci2011, 20, 168–178. [PubMed: 21082721]

(21). Laniado J; Yeates TOA Complete Rule Set for Designing Symmetry Combination Materials from Protein Molecules. Proc. Natl. Acad. Sci. U. S. A2020, 117, 31817–31823. [PubMed: 33239442]

(22). Simon AJ; Zhou Y; Ramasubramani V; Glaser J; Pothukuchy A; Gollihar J; Gerberich JC; Leggere JC; Morrow BR; Jung C; Glotzer SC; Taylor DW; Ellington ADSupercharging Enables Organized Assembly of Synthetic Biomolecules. Nat. Chem2019, 11, 204–212. [PubMed: 30643229]

(23). Lanci CJ; MacDermaid CM; Kang S-G; Acharya R; North B; Yang X; Qiu XJ; DeGrado WF; Saven JGComputational Design of a Protein Crystal. Proc. Natl. Acad. Sci. U. S. A2012, 109, 7304–7309. [PubMed: 22538812]

(24). Jeliazkov JR; Robinson AC; García-Moreno EB; Berger JM; Gray JJToward the Computational Design of Protein Crystals with Improved Resolution. Acta Crystallogr. Sect. D Struct. Biol2019, 75, 1015–1027. [PubMed: 31692475]

(25). Chen Z; Johnson MC; Chen J; Bick MJ; Boyken SE; Lin B; De Yoreo JJ; Kollman JM; Baker D; DiMaio FSelf-Assembling 2D Arrays with *de novo* Protein Building Blocks. J. Am. Chem. Soc2019, 141, 8891–8895. [PubMed: 31050411]

(26). Pyles H; Zhang S; De Yoreo JJ; Baker DControlling Protein Assembly on Inorganic Crystals through Designed Protein Interfaces. Nature2019, 571, 251–256. [PubMed: 31292559]

(27). Ben-Sasson AJ; Watson JL; Sheffler W; Johnson MC; Bittleston A; Somasundaram L; Decarreau J; Jiao F; Chen J; Mela I; Drabek AA; Jarrett SM; Blacklow SC; Kaminski CF; Hura GL; De Yoreo JJ; Kollman JM; Ruohola-Baker H; Derivery E; Baker DDesign of Biologically Active Binary Protein 2D Materials. Nature2021, 589, 468–473. [PubMed: 33408408]

(28). Bai Y; Luo Q; Liu JProtein Self-Assembly via Supramolecular Strategies. Chem. Soc. Rev2016, 45, 2756–2767. [PubMed: 27080059]

(29). Alex JM; Rennie ML; Volpi S; Sansone F; Casnati A; Crowley PBPhosphonated Calixarene as a “Molecular Glue” for Protein Crystallization. Cryst. Growth Des2018, 18, 2467–2473.

(30). Engilberge S; Rennie ML; Dumont E; Crowley PBTuning Protein Frameworks via Auxiliary Supramolecular Interactions. ACS Nano2019, 13, 10343–10350. [PubMed: 31490058]

(31). Alex JM; Guagnini F; Ramberg KO; Engilberge S; Crowley PBMolecular Glues for Protein Assembly. In Supramolecular Protein Chemistry: Assembly, Architecture and Application; Crowley PB, Ed.; The Royal Society of Chemistry: London, 2021; pp 199–232.

(32). Hu R; Yang G; Chen GThe Inducing Ligand Strategy for Supramolecular Protein Assembly. In Supramolecular Protein Chemistry: Assembly, Architecture and Application; Crowley PB, Ed.; The Royal Society of Chemistry: London, 2021; pp 233–257.

(33). Mirkin CA; Letsinger RL; Mucic RC; Storhoff JJA DNA-Based Method for Rationally Assembling Nanoparticles into Macroscopic Materials. Nature1996, 382, 607–609. [PubMed: 8757129]

(34). Macfarlane RJ; Lee B; Jones MR; Harris N; Schatz GC; Mirkin CANanoparticle Superlattice Engineering with DNA. Science2011, 334, 204–208. [PubMed: 21998382]

(35). Laramy CR; O’Brien MN; Mirkin CACrystal Engineering with DNA. Nat. Rev. Mater2019, 4, 201–224.

(36). He Y; Ye T; Su M; Zhang C; Ribbe AE; Jiang W; Mao CHierarchical Self-Assembly of DNA into Symmetric Supramolecular Polyhedra. Nature2008, 452, 198–201. [PubMed: 18337818]

(37). Zheng J; Birktoft JJ; Chen Y; Wang T; Sha R; Constantinou PE; Ginell SL; Mao C; Seeman NCFrom Molecular to Macroscopic via the Rational Design of a Self-Assembled 3D DNA Crystal. Nature2009, 461, 74–77. [PubMed: 19727196]

(38). Liu W; Tagawa M; Xin HL; Wang T; Emamy H; Li H; Yager KG; Starr FW; Tkachenko AV; Gang ODiamond Family of Nanoparticle Superlattices. Science2016, 351, 582–586. [PubMed: 26912698]

(39). Liu W; Halverson J; Tian Y; Tkachenko AV; Gang OSelf-Organized Architectures from Assorted DNA-Framed Nanoparticles. Nat. Chem2016, 8, 867–873. [PubMed: 27554413]

(40). Brodin JD; Auyeung E; Mirkin CADNA-Mediated Engineering of Multicomponent Enzyme Crystals. Proc. Natl. Acad. Sci. U. S. A2015, 112, 4564–4569. [PubMed: 25831510]

(41). McMillan JR; Brodin JD; Millan JA; Lee B; Olvera de la Cruz M; Mirkin CAModulating Nanoparticle Superlattice Structure Using Proteins with Tunable Bond Distributions. J. Am. Chem. Soc2017, 139, 1754–1757. [PubMed: 28121437]

(42). McMillan JR; Mirkin CADNA-Functionalized, Bivalent Proteins. J. Am. Chem. Soc2018, 140, 6776–6779. [PubMed: 29799197]

(43). Hayes OG; McMillan JR; Lee B; Mirkin CADNA-Encoded Protein Janus Nanoparticles. J. Am. Chem. Soc2018, 140, 9269–9274. [PubMed: 29989807]

(44). McMillan JR; Hayes OG; Winegar PH; Mirkin CAProtein Materials Engineering with DNA. Acc. Chem. Res2019, 52, 1939–1948. [PubMed: 31199115]

(45). Mou Y; Yu J-Y; Wannier TM; Guo C-L; Mayo SLNature2015, 525, 230–233. [PubMed: 26331548]

(46). Kashiwagi D; Sim S; Niwa T; Taguchi H; Aida TJAm. Chem. Soc2018, 140, 26–29.

(47). Subramanian RH; Smith SJ; Alberstein RG; Bailey JB; Zhang L; Cardone G; Suominen L; Chami M; Stahlberg H; Baker TS; Tezcan FAACS Cent. Sci2018, 4, 1578–1586. [PubMed: 30555911]

(48). Xu Y; Jiang S; Simmons CR; Narayanan RP; Zhang F; Aziz A-M; Yan H; Stephanopoulos NACS Nano2019, 13, 3545–3554. [PubMed: 30835439]

(49). Stephanopoulos NHybrid Nanostructures from the Self-Assembly of Proteins and DNA. Chem2020, 6, 364–405.

(50). McCluskey JB; Clark DS; Glover DJFunctional Applications of Nucleic Acid-Protein Hybrid Nanostructures. Trends Biotechnol2020, 38, 976–989. [PubMed: 32818445]

(51). Winegar PH; Hayes OG; McMillan JR; Figg CA; Focia PJ; Mirkin CADNA-Directed Protein Packing within Single Crystals. Chem2020, 6, 1007–1017. [PubMed: 33709040]

(52). Goldstein IJ; Poretz RDIsolation, Physicochemical Characterization, and Carbohydrate-Binding Specificity of Lectins. In The Lectins: Properties, Functions, and Applications in Biology and Medicine; Leiner IE, Sharon N, Goldstein IJ, Eds.; Academic Press: London, 1986; pp 35–250.

(53). Parkin S; Rupp B; Hope HAtomic Resolution Structure of Concanavalin A at 120 K. Acta Crystallogr., Sect. D: Biol. Crystallogr1996, 52, 1161–1168. [PubMed: 15299577]

(54). van Dun S; Ottmann C; Milroy L-G; Brunsveld LSupramolecular Chemistry Targeting Proteins. J. Am. Chem. Soc2017, 139, 13960–13968. [PubMed: 28926241]

(55). Supramolecular Protein Chemistry; Crowley PB, Ed.; Monographs in Supramolecular Chemistry; The Royal Society of Chemistry: London, 2021.

(56). Berman HMThe Protein Data Bank. Nucleic Acids Res2000, 28, 235–242. [PubMed: 10592235]

(57). Dotan N; Arad D; Frolow F; Freeman ASelf-Assembly of a Tetrahedral Lectin into Predesigned Diamondlike Protein Crystals. Angew. Chem., Int. Ed1999, 38, 2363–2366.

(58). Sakai F; Yang G; Weiss MS; Liu Y; Chen G; Jiang MProtein Crystalline Frameworks with Controllable Interpenetration Directed by Dual Supramolecular Interactions. Nat. Commun2014, 5, 4634. [PubMed: 25144207]

(59). Yang G; Kochovski Z; Ji Z; Lu Y; Chen G; Jiang MThree-Dimensional Protein Assemblies Directed by Orthogonal Non-Covalent Interactions. Chem. Commun2016, 52, 9687–9690.

(60). Hu R; Yang G; Ding HM; Ma J; Ma YQ; Gan J; Chen GCompetition between Supramolecular Interaction and Protein-Protein Interaction in Protein Crystallization: Effects of Crystallization Method and Small Molecular Bridge. Ind. Eng. Chem. Res2018, 57, 6726–6733.

(61). Yan H; Aguilar AL; Zhao YPreparation of Carbohydrate-Oligonucleotide Conjugates Using the Squarate Spacer. Bioorg. Med. Chem. Lett2007, 17, 6535–6538. [PubMed: 17935985]

(62). Hou S-J; Saksena R; Kováč PPreparation of Glycoconjugates by Dialkyl Squarate Chemistry Revisited. Carbohydr. Res2008, 343, 196–210. [PubMed: 18048016]

(63). Wurm FR; Klok HABe Squared: Expanding the Horizon of Squaric Acid-Mediated Conjugations. Chem. Soc. Rev2013, 42, 8220–8236. [PubMed: 23873344]

(64). Marchetti LA; Kumawat LK; Mao N; Stephens JC; Elmes RBPThe Versatility of Squaramides: From Supramolecular Chemistry to Chemical Biology. Chem2019, 5, 1398–1485.

(65). Dean BR; Homer RBThe Use of a Fluorescently Labelled Sugar to Investigate Binding by Concanavalin A. Biochim. Biophys. Acta, Protein Struct1973, 322, 141–144.

(66). Loontiens FG; Clegg RM; Jovin TMBinding of 4-Methylumbelliferyl $\alpha$-D-Mannopyranoside to Tetrameric and Unmodified or Derivatized Dimeric Concanavalin A: Equilibrium Studies. Biochemistry1977, 16, 159–166. [PubMed: 836781]

(67). Dessau MA; Modis YProtein Crystallization for X-Ray Crystallography. J. Visualized Exp2011, 47, e2285.

(68). Viladoms J; Parkinson GNHELIX: A New Modular Nucleic Acid Crystallization Screen. J. Appl. Crystallogr2014, 47, 948–955.

(69). Ussery DWDNA Structure: A-, B- and Z-DNA Helix Families. In Encyclopedia of Life Sciences; John Wiley & Sons, Ltd: Chichester, UK, 2002; pp 1–7, DOI: 10.1038/npg.els.0003122.

(70). Naismith JH; Emmerich C; Habash J; Harrop SJ; Helliwell JR; Hunter WN; Raftery J; Kalb AJ; Yariv JRefined Structure of Concanavalin A Complexed with Methyl $\alpha$-DMannopyranoside at 2.0 Å Resolution and Comparison with the Saccharide-Free Structure. Acta Crystallogr., Sect. D: Biol. Crystallogr1994, 50, 847–858. [PubMed: 15299352]

(71). Loris R; Maes D; Poortmans F; Wyns L; Bouckaert JA Structure of the Complex between Concanavalin A and Methyl-3,6-Di-O-(α-D-Mannopyranosyl)-$\alpha$-D-Mannopyranoside Reveals Two Binding Modes. J. Biol. Chem1996, 271, 30614–30618. [PubMed: 8940035]

(72). Kadirvelraj R; Foley BL; Dyekjær JD; Woods RJInvolvement of Water in Carbohydrate–Protein Binding: Concanavalin A Revisited. J. Am. Chem. Soc2008, 130, 16933–16942. [PubMed: 19053475]

(73). Trastoy B; Bonsor DA; Pérez-Ojeda ME; Jimeno ML; Méndez-Ardoy A; Manuel García Fernández J; Sundberg EJ; Chiara JLSynthesis and Biophysical Study of Disassembling Nano Hybrid Bioconjugates with a Cubic Octasilsesquioxane Core. Adv. Funct. Mater2012, 22, 3191–3201.

(74). Krissinel E; Henrick KInference of Macromolecular Assemblies from Crystalline State. J. Mol. Biol2007, 372, 774–797. [PubMed: 17681537]

(75). Sanders DA; Moothoo DN; Raftery J; Howard AJ; Helliwell JR; Naismith JHThe 1.2 Å Resolution Structure of the Con A-Dimannose Complex. J. Mol. Biol2001, 310, 875–884. [PubMed: 11453694]

(76). Zhang Z; Qian M; Huang Q; Jia Y; Tang Y; Wang K; Cui D; Li MCrystal Structure of the Complex of Concanavalin A and Tripeptide. J. Protein Chem2001, 20, 59–65. [PubMed: 11330349]

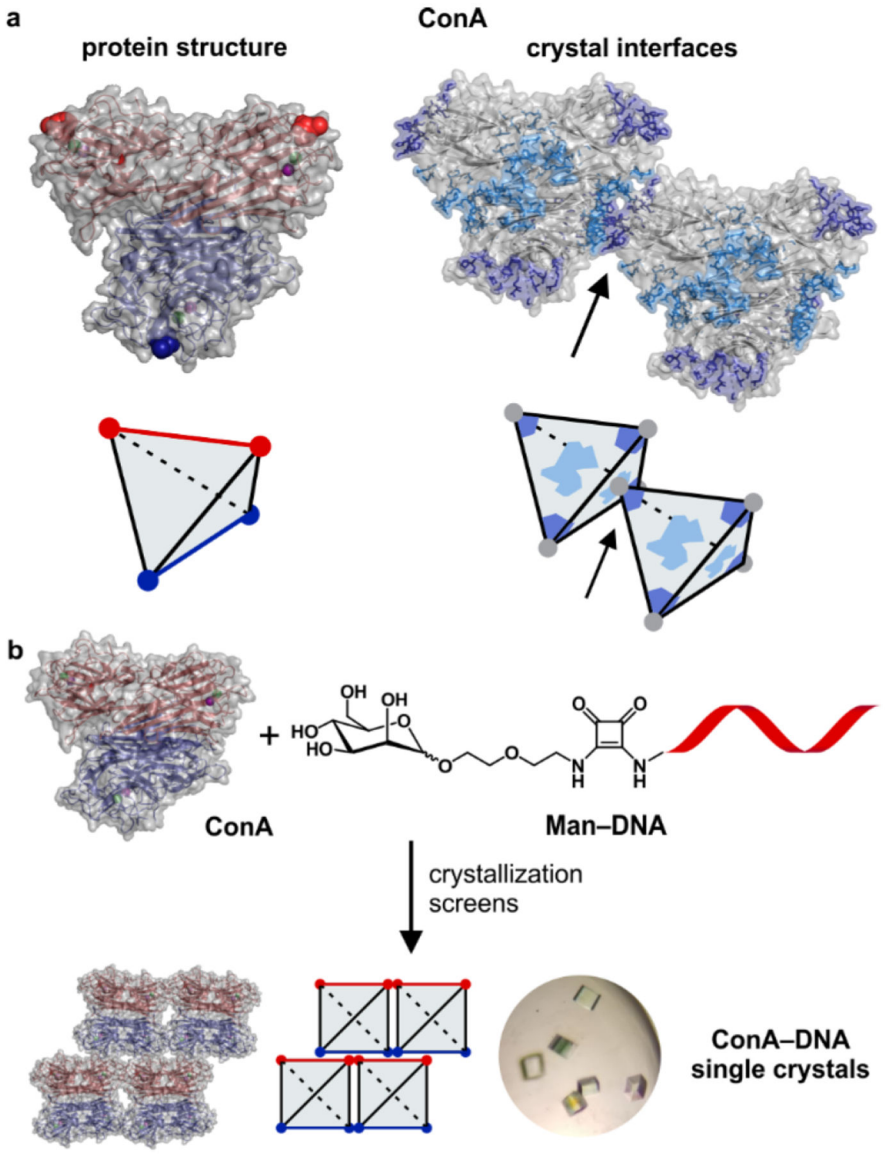


**Scheme 1. Crystallization of Concanavalin A (ConA) with DNA[a]**

[a](a) ConA is a homotetramer with an approximately tetrahedral topology. (Left) Tetrahedral ConA binds mannose through four binding sites at its vertices (red and blue). For ease of visualization, two amino acid chains are colored in red and two are colored in blue. (Right) In its native crystal packing (PDB: 1JBC[53]), the major interface between tetramers exists between the vertex of one tetramer (dark blue) and the face of another tetramer (light blue). (b) Mixtures of ConA and a mannose-containing DNA glycoconjugate (Man-DNA) were crystallized in high-throughput screens. (Bottom) Crystals are represented as (left to right) molecular structures, schematic depictions, and optical microscope images.

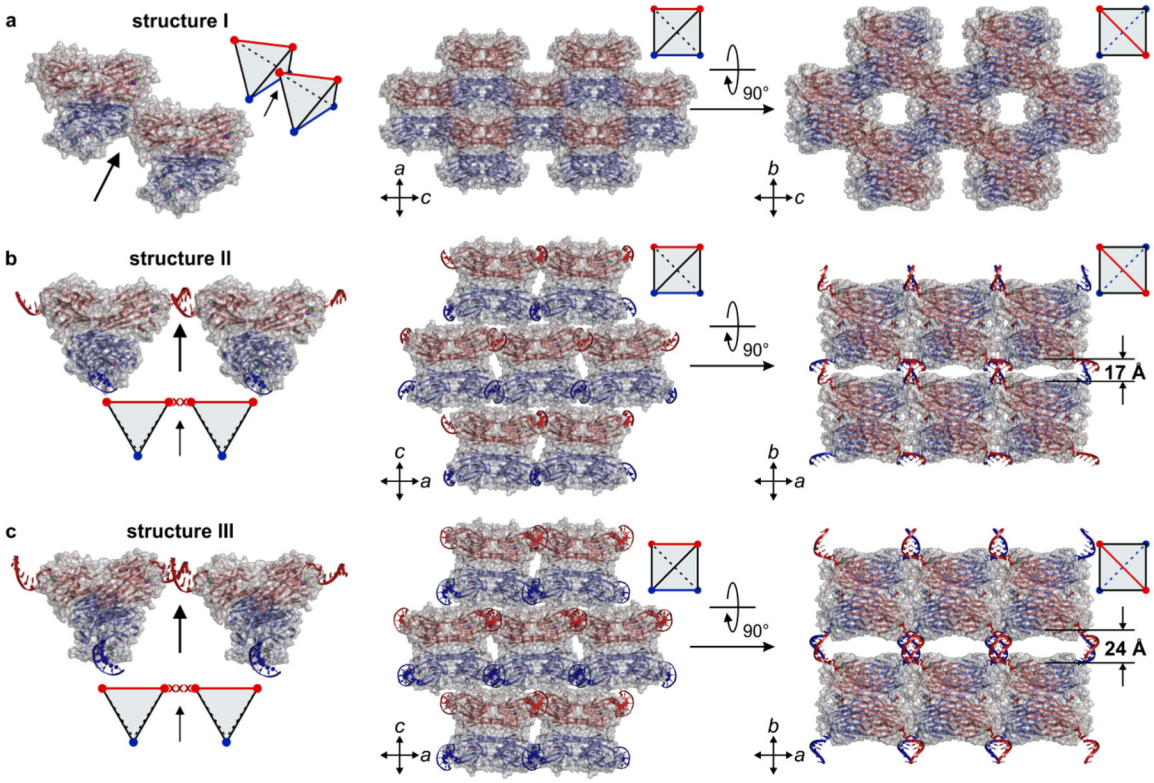


**Figure 1.**

Crystal structures of ConA with 5′-Man–DNA glycoconjugates. (a) Native ConA crystallizes into structure I, in which (left) the major interaction between tetramers occurs via a vertex–face interface, denoted by an arrow. Proteins are arranged in (center) densely packed sheets that give a (right) porous structure. (b, c) When mixed with complementary or self-complementary Man–DNA glycoconjugates, ConA crystallizes into two novel packings defined by DNA length: (b) structure II, 4-bp DNA, and (c) structure III, 6-bp DNA. In these structures, (left) DNA defines the primary interaction between two tetramers (denoted by an arrow). Proteins assemble into (center) staggered sheets that stack via (right) DNA interactions. Distances noted in b, c (right) are measured between the C$\alpha$ atoms of two D78 residues.

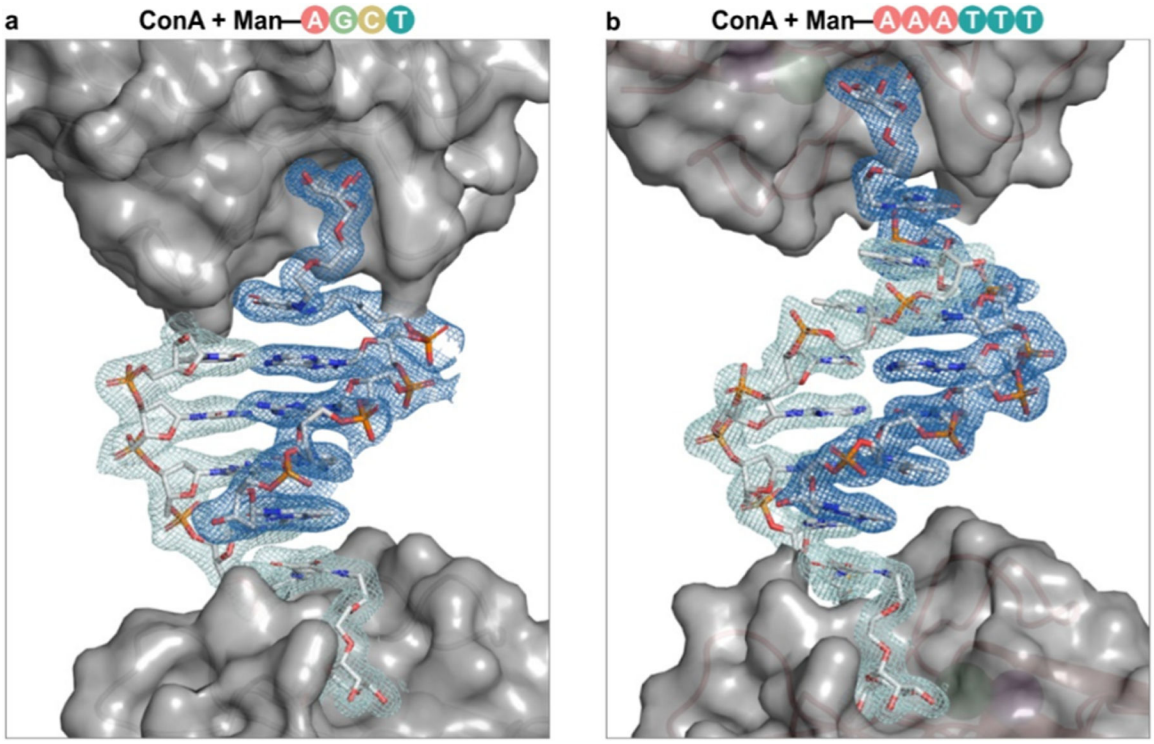


**Figure 2.**

Conformation of DNA in ConA-DNA single crystals. DNA glycoconjugates in crystal structures of ConA with (a) Man-AGCT and (b) Man-AAATTT adopt nearly identical conformations and protrude from the mannose-binding site in the same direction. Difference maps comparing electron density observed experimentally and calculated from a protein-only model ($F_o - F_c$) show substantial unmodeled electron density. This density correlates closely with a double helix of B-form DNA.[69] $F_o - F_c$ maps are depicted at 1.0 $\sigma$ in light and dark blue.

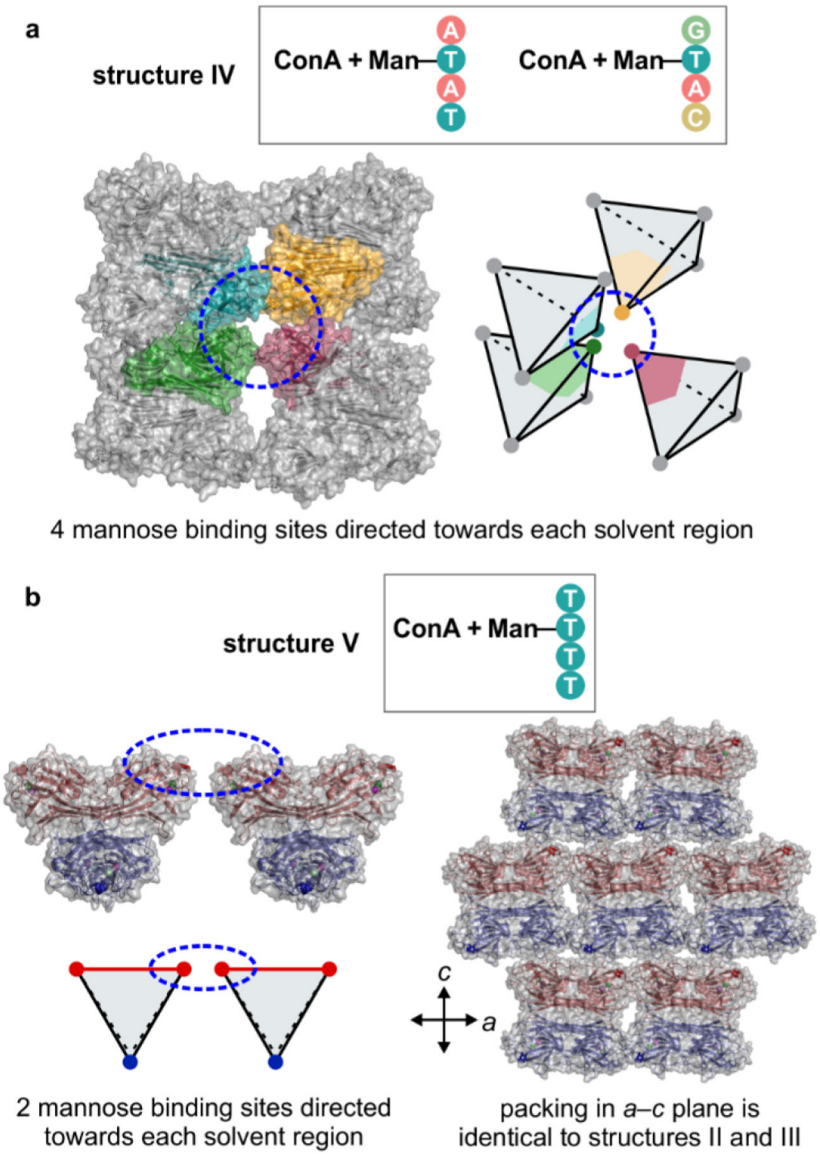


**Figure 3.**

Crystal structures of ConA with internally modified DNA glycoconjugates. (a) ConA crystallizes with self-complementary internally modified 4-bp DNA (A(Man-T)AT, G(Man-T)AC) into a novel packing, structure IV. In this crystal, regions of solvent space are surrounded by the mannose-binding sites of four ConA tetramers. (b) Crystals of ConA with a noncomplementary analogue (T(Man-T)TT) were solved into a distinct structure, structure V, in which regions of solvent space are surrounded by the mannose-binding sites of two ConA tetramers. Within structure V, proteins pack into staggered sheets identical to those observed in structures II and III (Figure 1b,c, center).

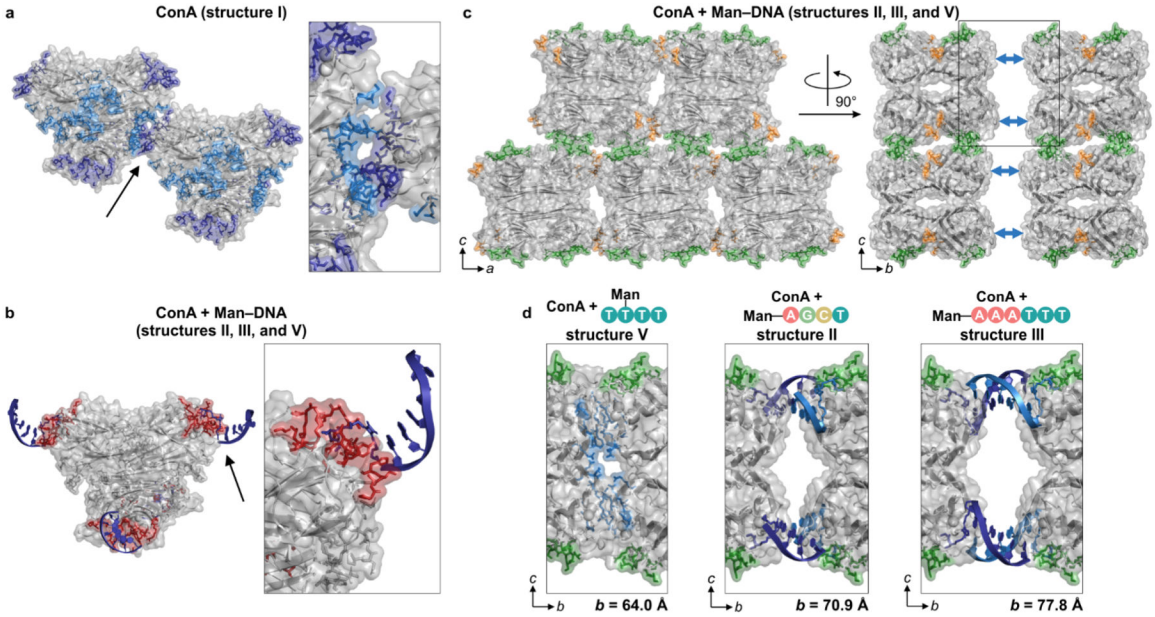


**Figure 4.**

Interface analysis of ConA-DNA single crystals. (a) In native ConA crystals (structure I), the major interface between tetramers exists between the vertex of one tetramer (surface residues in dark blue) and the face of another tetramer (light blue). (b) Upon binding, Man-DNA (dark blue) sterically blocks the surface residues surrounding the mannose-binding site (red), thus eliminating the predominant interaction in structure I. (c) ConA packs into identical, staggered layers in structures II, III, and V. ConA tetramers interact via orthogonal interfaces along the *c*and *a*-directions (surface residues in green and orange, respectively). The structures differ only in their interactions along the *b*-direction (blue arrows). (d) DNA design leads to specific changes in the interaction between ConA tetramers along the *b*-direction. In structure V, there are no complementary DNA interactions, and thus proteins interact via PPIs (surface residues in blue). In structures II and III, interactions between proteins along the *b*-direction are defined by self-complementary DNA–DNA interactions, with a corresponding increase in the unit cell parameter *b* with increasing DNA length.

**Table 1.**

Summary of Crystal Properties for ConA–DNA Single Crystals

| sample | PDB code | structure | space group | *a*, *b*, *c* (Å)[a] | resolution (Å) |
|---|---|---|---|---|---|
| ConA + no DNA | 7MG1 | I | *I*222 | 61.19, 85.18, 89.25 | 2.00 |
| ConA + **Man-8** | 7MG2 | I | *I*222 | 61.42, 86.13, 89.50 | 1.80 |
| ConA + ATAT | 7MG3 | I | *I*222 | 62.07, 86.39, 89.32 | 1.60 |
| ConA + Gal-ATAT | 7MG4 | I | *I*222 | 61.63, 86.03, 89.23 | 2.00 |
| ConA + Man-ATAT | 7MG5 | II | $P2_122_1$ | 65.69, 70.70, 125.87 | 2.10 |
| ConA + Man-AGCT | 7MG6 | II | $P2_122_1$ | 65.73, 70.89, 125.84 | 1.70 |
| ConA + Man-GTAC | 7MG7 | II | $P2_122_1$ | 65.87, 70.40, 125.09 | 1.75 |
| ConA + Man-CGCG | 7MG8 | II | $P2_122_1$ | 66.42, 69.92, 125.87 | 3.00 |
| ConA + Man-TTTT + Man-AAAA | 7MG9 | II | $P2_122_1$ | 65.98, 70.18, 124.42 | 2.55 |
| ConA + Man-TTTT | – | – | – | – | – |
| ConA + Man-AAATTT | 7MGA | III | $P2_122_1$ | 65.09, 77.78, 126.06 | 2.00 |
| ConA + A(Man-T)AT | 7MGB | IV | $P22_12_1$ | 68.01, 117.48, 122.49 | 2.45 |
| ConA + G(Man-T)AC | 7MGC | IV | $P22_12_1$ | 69.33, 117.34, 122.40 | 2.92 |
| ConA + T(Man-T)TT | 7MGD | V | $P12_11$ | 60.56, 63.97, 126.45[b] | 2.05 |

[a] Unless otherwise noted, $\alpha = \beta = \gamma = 90.00°$. – denotes that the sample did not crystallize.

[b] $\alpha = \gamma = 90.00°$, $\beta = 93.30°$.